

SCG060-P01

Room:Convention Hall

Time:May 25 16:15-18:45

## Understanding the dynamics of thermo-chemical mantle wedge based on a simple model

Satoru Honda<sup>1\*</sup>, Taras Gerya<sup>2</sup>, Guizhi Zhu<sup>2</sup>

<sup>1</sup>ERI, Univ. Tokyo, <sup>2</sup>ETH Zurich

Complex dynamical phenomena may be expected in the mantle wedge, since it will be controlled by a combination of thermal and chemical effects. Recent our studies show the possibility of the existence of small-scale convection in the mantle wedge, which may be driven by thermal/chemical buoyancies. Such a small-scale convection may explain the along-arc variation of arc volcanism. In order to understand the complex phenomena associated with thermal and chemical effects, we have constructed a simplified model of thermo-chemical convection in the mantle wedge. In this model, we assume the kinematic flow of a chemical agent, such as water, from the top of the subducting slab. This chemical agent affects both the density and the viscosity of the region where it resides and decreases the density and viscosity.

We found that major effects of this low density and viscosity anomaly is to suppress the three-dimensional characteristic of mantle flow. Chemically polluted, thus buoyant region tends to stagnate and this results in the low temperature zone in the corner of mantle wedge. This result suggests the chemical origin of non-moving mantle part in the corner of the mantle wedge (nose), which is sometimes necessary to explain the low heat flow in the fore-arc. We also constructed a hybrid model: The chemical agency close to the trench affects both density and viscosity and it in the back arc region does only the viscosity. The model shows the co-existence of the low temperature nose and the small-scale thermally driven convection in the back arc. This may explain some of the geologic character of the northern Honshu arc.

Keywords: subduction zone, small-scale convection, water, arc volcanism

## Depth Dependence of Subduction Zone Seismicity and its Uniformity

Keiko Kuge<sup>1\*</sup>

<sup>1</sup>Dept. Geophysics, Kyoto University

Arc volcanoes are typically located where the subducting slab is ~110 km deep (e.g. Tatsumi, 1986). To explain the uniformity of the arc volcano configuration, Wada and Wang (2009) proposed subduction zone thermal models with common decoupling depth, in which the interface between the slab and the mantle wedge is decoupled to a depth of 70-80 km where mantle wedge flows are not dragged by the subducting slab. If the thermal models really dominate, not only thermal structure but also earthquake activity in subduction zones can be affected because the condition of temperature controls seismogenesis at plate boundaries and within slabs. In this study, I attempt to diagnose the models of Wada and Wang (2009) by examining variation of seismic activity with depth in subduction zones.

Using earthquake hypocenter data relocated by the method of Engdahl et al. (1998), I examine dependence of earthquake frequency on depth down to 200 km. In subduction zones with thermal parameters larger than 800 km, the number of earthquakes exponentially decreases with depth below ~50 km, and the decreasing rate changes at depth of 75-100 km. The depth changing the decreasing rate seems to be uniform in the subduction zones, having no significant correlation with the thermal parameters. Depth distribution of earthquakes deeper than 75-100 km tends to depend on subduction zones. In some subduction zones the earthquake frequencies continue to be at low rates, whereas there are dominant peaks of earthquake activity at depths in some subduction zones. The similar observations are also obtained in the Global CMT catalogue.

Using the Global CMT catalog, I examine the depth distribution of earthquakes which depends on focal mechanisms. The depth of 75-100 km is close to the lower limit where thrust earthquakes occur. Low-angle thrust earthquakes, which may be plate-boundary earthquakes, occur at depths shallower than 75 km. My waveform modeling for some low-angle thrust earthquakes shows that the depths are shallower than ~50km. The depth of 75-100 km is a turning depth where focal mechanisms change. Therefore, change in earthquake frequency at depth of 75-100 km can be a manifestation of two features: Vanishing of thrust earthquakes above 75 km and no significant increase of slab earthquakes at depths of 75-100 km shallower. Taking account of the dependence of the two features on temperature, the uniformity observed for the variation of seismic activity with depth in subduction zones is consistent with the thermal models of Wada and Wang (2009).

SCG060-P03

Room:Convention Hall

Time:May 25 16:15-18:45

## Major and Trace elements mineral composition in peridotites from the Ust'-Belaya ophiolite, Far East Russia

Sumiaki Machi<sup>1\*</sup>, Akira Ishiwatari<sup>2</sup>, Tomoaki Morishita<sup>3</sup>, Yasutaka Hayasaka<sup>4</sup>, Galina V. Ledneva<sup>5</sup>, Borys A. Bazylev<sup>5</sup>, Sergei D. Sokolov<sup>5</sup>, Suren A. Palandzhyan<sup>5</sup>, Akihiro Tamura<sup>3</sup>, Shoji Arai<sup>6</sup>

<sup>1</sup>Natural Sci. & Tec., Kanazawa Univ., <sup>2</sup>NE Asia Center, Tohoku Univ., <sup>3</sup>FSO, Kanazawa Univ., <sup>4</sup>Earth & Planet. Sys. Sci., Hiroshima Uni., <sup>5</sup>Geol. Inst. Russia Academy of Science, <sup>6</sup>Earth Sci. Course, Kanazawa Univ.

The Ust'-Belaya ophiolite is exposed in the 80 km x 40 km area on the south of Ust'-Belaya (N65 30', E173 17'), Far East Russia (Sokolov et al., 2003, Geol. Soc. London, Spec. Publ., 218, 619-). The associated limestone suggests Devonian or older age of this ophiolite. It is an important character of this ophiolite that glaucophane-bearing rocks occur. Here we report the petrographical features and mineral chemistry of the peridotite from the Ust'-Belaya ophiolite and discuss about their metamorphism and metasomatism.

Mantle section of the Ust'-Belaya ophiolite is composed of fertile lherzolite to moderately depleted harzburgite. As a result of significant hydration, those peridotites contain various hydrous minerals such as amphibole, talc, secondary clinopyroxene and antigorite. In some of antigorite-bearing peridotites, olivine shows an apparent "cleavage". Such petrographical characteristics resemble those of the antigorite-bearing serpentinite from Mariana forearc (Ohara & Ishii, 1998, Island Arc, 7, 541-; Murata et al., 2009, Geosphere, 5, 90-).

Cr# of spinel in the Ust'-Belaya peridotite shows wide range from 0.1 to 0.5, which is similar compositional range to these of the mid ocean ridge peridotites. It is noteworthy that low-Cr spinel (Cr#=0.1) coexist with high-Na clinopyroxene. Such Na-cpx shows similar trace element pattern to the mid ocean ridge peridotite, which is explained by simple extraction of melts. Therefore such Na-rich clinopyroxene bearing peridotite may represent the deeper level of melting column. On the other hand, the other clinopyroxenes show LREE-enriched trace elements patterns, which is cannot be explained by simple extraction of melts. These patterns can be explained by influx melting.

Amphiboles show different compositional trend corresponding to the mineral assemblage. In Atg-free type rocks, amphibole covers a compositional range from tremolite to pargasite. Meanwhile, in Atg-bearing type rocks, amphibole covers a compositional range from tremolite to richterite with edenite. Trace elements patterns of the former amphiboles (magnesiohornblende) are similar to those of clinopyroxenes in the same sample. Therefore the fluid related to the influx melting was able to be responsible for the formation of these amphiboles. On the other hand, the latter amphiboles (Na-rich tremolite/richterite) shows low concentration and pronounced positive anomaly for Sr. This indicate introduction of Na and Sr coupled with removal of these elements.

The influx melting inferred from trace elements patterns of cpx, as well as the occur of glaucophane-bearing rocks, low equilibrium temperature of peridotites and the evidence of fluid-peridotite interaction are suggesting the Ust'-Belaya peridotite may represent a fragment of the pre-late Paleozoic forearc mantle wedge. Absence of highly depleted peridotite suggests that highly depleted peridotites are not necessary for every forearc environments.

Keywords: subduction zone, antigorite, amphibole, serpentinization

SCG060-P04

Room:Convention Hall

Time:May 25 16:15-18:45

## XANES study on the redox state of silicate glasses in: a preliminary result for boninites from Ogasawara Islands, Japan

Hidemi Ishibashi<sup>1\*</sup>, Shoko Odake<sup>1</sup>, Hiroyuki Kagi<sup>1</sup>

<sup>1</sup>Geochemical Research Center, Univ. Tokyo

The redox state of arc mantle is not only of geochemical interest but also an important factor to understand processes of material cycle and generation of arc magma within mantle wedge. Previous studies on mantle xenoliths indicated that arc mantle is more oxidized relative to those of other tectonic settings and proposed that the oxidized nature is attributed to an influence of subduction-related fluid. However, it is unobvious that partially melted region within mantle wedge where arc magma is generated is actually oxidized because mantle xenoliths are fragments of cool, rigid, re-equilibrated lithospheric mantle. In addition, the role of subduction-related fluid on oxidization of arc mantle is still unclear.

Arc magmas might be a unique material having information about the redox state of their source mantle region. Among various arc magmas, we thought that boninite is most suitable to examine both the redox state of arc mantle and the effect of subduction-related fluid. This is because they are undifferentiated and their modification during ascent was minimal. In addition, they were considered to be generated by partial melting of hydrous mantle which was highly influenced by subduction-related fluid. Therefore, the redox state of boninite is expected to have a key to clarify above issues.

It is well known that valence state of Fe in silicate glass is a sensitive indicator of its oxygen fugacity ( $fO_2$ ) and can be determined from pre-edge feature in Fe K-edge XANES spectrum. In this study, we investigated  $fO_2$  of silicate glasses included in three boninite pillow lavas from Chichijima and Mukojima, Ogasawara islands, Japan, using Fe K-edge micro X-ray absorption near-edge structure (XANES) spectroscopy. A natural glass included in pahoehoe lava from Kilauea volcano, Hawaii was also analyzed for comparison. We performed the measurements using Beam Line 4A in Photon Factory, KEK, which enables us micro analysis of XANES. The obtained spectra were analyzed using the method of Cottrell et al. (2009). Two pre-edge peaks centered at ca. 7112eV (peak-1) and ca. 7114eV (peak-2), respectively, are commonly observed for silicate glass. The former and the latter are attributed to absorptions by Fe<sup>2+</sup> and Fe<sup>3+</sup> in silicate glass, respectively, and intensity ratio of peak-2 to peak-1 increases with increasing Fe<sup>3+</sup>/Fe<sup>2+</sup> ratio. Therefore, the intensity ratio is a useful indicator of  $fO_2$  for silicate glass. We estimate  $fO_2$  of silicate glass using the relation between the intensity ratio and  $fO_2$  based on experimental dataset for basaltic glass (Cottrell et al. 2009).

We measured several points of groundmass glasses for each lava samples and confirmed that groundmass glass is homogeneous in terms of Fe<sup>3+</sup>/Fe<sup>2+</sup> ratio for the studied samples. Delta QMF (Quartz-Magnetite-Fayalite) value [= log  $fO_2$ (sample) ? log  $fO_2$ (QMF buffer)] of +0.2 was obtained for Kilauea pahoehoe glass. This is consistent with previous studies, demonstrating reliability of this method. Delta QMF values are +0.7 for a samples from Chichijima and +0.5 and +1.3 for two samples from Mukojima, respectively. With considering the fact that the intensity ratio is higher for silicic glass than for basaltic glass at the same Fe<sup>2+</sup>/Fe<sup>3+</sup> ratio and boninite is more enriched in SiO<sub>2</sub> than basalt, the boninites may be more reduced than the estimated  $fO_2$  conditions. In addition, previous study showed that crystallization of mafic silicate minerals slightly oxidizes silicate melt and the effect of dehydration during ascent on  $fO_2$  of silicate melt is negligible. This suggests that the redox condition of primially boninite melt, and hence of its source mantle, was at least more reduced than the estimated  $fO_2$  (near QMF buffer) whereas it was highly influenced by subduction-related fluid. Therefore, the effect of subduction-related fluid on the redox state of partially melted arc mantle is considered to be minor.

Keywords: XANES, arc mantle, boninite, redox state, oxygen fugacity, silicate glass

SCG060-P05

Room:Convention Hall

Time:May 25 16:15-18:45

## Partial melting in deep subduction zone detected from zircon preserved in the Sanbagawa eclogite

Miyuki Arakawa<sup>1\*</sup>, Kazuaki Okamoto<sup>1</sup>, Yukiyasu Tsutsumi<sup>2</sup>, Terabayashi Masaru<sup>3</sup>

<sup>1</sup>Saitama University,Japan, <sup>2</sup>National Science Museum, <sup>3</sup>Kagawa University,Japan

Subducting oceanic plate is dehydrated due to metamorphic reaction in higher pressure and temperature conditions. The dehydrated fluid is considered to cause deep focused earthquake and Island Arc volcanism. Recently we have discovered an eclogite outcrop exhibiting partial melting texture from the Sanbagawa high P/T metamorphic belt, characterized as subducted oceanic material (Okamoto & Arakawa, 2011). The discovery is significantly important because the melt may play an important role in deep-focused earthquake and the melt itself directly may contribute to the origin of Island Arc magma. Due to an extensive retrograde hydration and deformation, melting process is only preserved in garnet on thin section. Zircon is the best tool to reconstruct melting process at eclogite facies condition because it preserves 1) high P minerals, 2) melt and fluid as inclusion and 3) the zircon growth history can be traced from its zonal texture.

### Analytical method

We carefully collected the eclogite (SHT15) and the melted portion (SHT16) characterized as quartz-plagioclase rich domain from the outcrop exhibiting melting texture. Zircon separation was based on Tsutsumi et al. (2009). One another sample (SHT17) showing the eclogite with minor melted texture was also collected. Separated zircons from the above three specimens were carefully observed under SEM, CL, and the zircon inclusions were identified using EDS and laser Raman.

### Result

The zircons from the eclogite portion (SHT15) are elongated and have relatively large diameters in 100 to 250 microns. The zircons from the melted portion (SHT16) are rounded and 100 to 200 microns. The specimens SHT17 have elongated and rounded zircons. Zonal textures in the zircon from the SHT15 are classified as core, mantle and rims. Zircons from the melted portion (SHT16) have homogeneous core with thin mantle and rims. Zircon inclusions from the core (SHT15 and SHT17) are characterized as igneous and altered phase (apatite and gypsum). Rutile and amphibole are recognized from the mantle.

### Discussion and conclusion

The zircon features from the melted portion (SHT16) are identical with the zircons (GO4) from the quartz bearing eclogite described by Okamoto et al. (2004). The GO4 zircons are considered as grown at prograde stage (120 to 110 Ma). The zircons from the SHT15 and SHT17 are comparable with zircons from the metasedimentary rock (QM) associated with the quartz bearing eclogite (Okamoto et al. 2004). The QM zircons have detrital core with metamorphic mantle grown at 120-110 Ma and thin rims. These lines of evidence suggest that the Sanbagawa eclogite suffered partial melting in deep subduction zone. Under the micron scope, mylonite texture is obvious in thin sections from the specimen SHT16. It may suggest that semi-brittle deformation was caused by partial melting and the melt accumulation was also governed by the deformation.

Keywords: deep subduction zone, partial melting, eclogite, zircon

SCG060-P06

Room:Convention Hall

Time:May 25 16:15-18:45

## Velocity and conductivity measurements on synthetic wet halite rocks at high pressure and temperature

Tohru Watanabe<sup>1\*</sup>, Motoki Kitano<sup>1</sup>

<sup>1</sup>University of Toyama

Intercrystalline fluid can significantly affect rheological and transport properties of rocks. Its influences are strongly dependent on its distribution. The dihedral angle between solid and liquid phases has been widely accepted as a key parameter that controls solid-liquid textures. The liquid phase is not expected to be interconnected if the dihedral angle is larger than 60 degree. However, observations contradictory to dihedral angle values have been reported. Watanabe and Peach (2002) suggested the coexistence of grain boundary brine with a positive dihedral angle. For good understanding of fluid distribution, it is thus critical to study the nature of grain boundary fluid.

We have developed a high pressure and temperature apparatus for study of intercrystalline fluid distribution. It was specially designed for measurements of elastic wave velocities and electrical conductivity. Elastic wave velocities ( $V_p$  and  $V_s$ ) and electrical impedance can be measured to constrain intercrystalline fluid distribution. The apparatus mainly consists of a conventional cold-seal vessel with an external heater. The pressure medium is silicon oil of the viscosity of 10 Pa s. The pressure and temperature can be controlled from 0 to 200 MPa and from 20 to 200 C, respectively. Dimensions of a sample are 9 mm in diameter, and 15 mm in length.

Halite-water system is used as an analog for crustal rocks. The dihedral angle has been studied systematically at various pressure and temperature conditions [Lewis and Holness, 1996]. The dihedral angle is larger than 60 degree at lower pressure and temperature. It decreases to smaller than 60 degree with increasing pressure and temperature. A sample is prepared by cold-pressing and annealing of wet NaCl powder. Optical examination has shown that synthesized samples are microstructurally homogeneous. Grains are polygonal and equidimensional with a mean diameter of 300 micrometer. Grain boundaries vary from straight to bowed and 120 degree triple junctions are common. Gas and fluid bearing inclusions are visible on the grain boundaries. There are spherical inclusions or isolated worm-like channels.

In this poster, we will report preliminary results of compressional wave velocity and electrical conductivity measurements.

Keywords: elastic wave velocity, electrical conductivity, halite, water



SCG060-P07

Room:Convention Hall

Time:May 25 16:15-18:45

## CO<sub>2</sub> bearing saline aqueous fluid inclusions in olivine of peridotite xenoliths of Pinatubo 1991 ejecta

yoshitaka kumagai<sup>1\*</sup>, Tatsuhiko Kawamoto<sup>1</sup>, Masako Yoshikawa<sup>1</sup>, Tetsuo Kobayashi<sup>2</sup>

<sup>1</sup>Inst. Geothermal Sci., Kyoto Univ., <sup>2</sup>Earth and Environ. Sci., Kagoshima Univ.

Spinel peridotite xenoliths are present in the dacitic rocks of the Pinatubo 1991 eruption, Luzon Island, Philippines. The Pinatubo volcano is one of the Bataan arc-front volcanoes that are associated with eastward subduction of the South China Sea floor along the Manila Trench. Peridotite xenoliths are mainly composed of olivine and orthopyroxene, with minor amounts of spinel and calcic amphibole surrounding spinel and orthopyroxene. Small grains of clinopyroxene and phlogopite also surround spinel and orthopyroxene. Phlogopite and amphibole inside of peridotite xenoliths have major element chemistry different from those of selvage.

Many fluid inclusions less than 30 micrometer in diameter are present in olivine. Raman spectroscopy shows that those fluid inclusions are mainly composed of H<sub>2</sub>O, magnesite, unidentified crystal and a bubble. Raman spectra indicate the presence of hydrous mineral on a wall of host olivine, which can be a talc. In addition to these phases, CO<sub>2</sub> is also found in vapor bubbles in inclusions. These suggest that the inclusions were composed of H<sub>2</sub>O-CO<sub>2</sub> and reacted with olivine to form talc, magnesite, and CO<sub>2</sub> - bearing aqueous fluids. Using a cooling stage, we determined melting temperature of ice and estimated NaCl equivalent amount dissolved in the fluid inclusions to be 5-14 weight %. This amount of NaCl is not strictly but roughly consistent with an estimation based on Raman spectra. Since the original fluids reacted with olivine after their capture, homogenization temperature without re-reaction involved of olivine, magnesite, talc, and fluids does not provide meaningful density of original fluids.

As a pioneer work, Roedder (1965, American Mineralogist) reported CO<sub>2</sub> inclusions commonly observed in mantle xenoliths in worldwide. One exception was CO<sub>2</sub>-H<sub>2</sub>O inclusion from orthopyroxene in a peridotite xenolith of Ichinome-gata, a back-arc side in the northeast Japan arc. For last 15 years, H<sub>2</sub>O inclusions have been reported from several peridotite xenoliths in subduction zones: from Iraya, Bataan (Schiano et al., 1995, Nature), Lihir, Papua New Guinea (McInnes et al., 2001, Earth and Planetary Science Letter) and Avacha, Kamchatka (Ishimaru and Arai, 2008, Geological Society, London, Special Publications). The present description of the fluid inclusions in the Pinatubo peridotites indicates that CO<sub>2</sub> bearing saline aqueous fluids are present beneath the volcanic front in Bataan arc, Philippines.

Keywords: water, fluid inclusion, carbonate, peridotite, mantle, Pinatubo volcano

SCG060-P08

Room: Convention Hall

Time: May 25 16:15-18:45

## Synthetic aqueous inclusions of dehydrated fluids from hydrated minerals

Shugo Ohi<sup>1\*</sup>, Tetsu Kogiso<sup>1</sup>, Akira Miyake<sup>2</sup>

<sup>1</sup>Kyoto university HES, <sup>2</sup>Kyoto university Science

### Introduction

Deep aqueous fluids derived from subducted plate significantly affect volcanic activity in the subduction zone. Therefore, it is important to examine the chemical compositions of dehydrated fluids from hydrated minerals to grasp H<sub>2</sub>O behavior in the subduction zone. However, quantitative estimations from material sciences for deep aqueous fluids were not discussed enough, whereas thermodynamic models were sufficiently discussed. The observation and analysis of aqueous fluids is needed to grasp deep aqueous fluids behavior in the subduction zone.

In natural samples, fluids were trapped in minerals. Purpose in present study is to trap dehydrated fluids from hydrated minerals in quartz single crystals.

### Previous studies

Sterner and Bodnar (1984) made synthetic fluid inclusions by using internally heated pressure vessels. They sealed quartz crystal with micro cracks and the desired fluid composition in noble metal capsules. Synthetic fluid inclusions were formed by healing fractures in natural quartz in their study. Since then, many researchers synthesized fluids inclusions. However, no one make synthetic aqueous inclusions of dehydrated fluids from hydrated minerals.

In the meanwhile, Kogiso et al. (1997) carried out dehydration experiments on a natural amphibolite under open system conditions. They estimated the chemical composition of aqueous fluid from the gap between starting amphibolite and dehydrated charge.

In present study, we trapped dehydrated fluid from hydrated minerals in quartz by using crack healing method.

### Experimental methods

Starting materials were Brazilian quartz single crystals and H<sub>2</sub>O and Mg(OH)<sub>2</sub>. Quartz single crystals were cut into about 1-2mm size and inclusion-free crystals were selected as starting materials. Inclusion-free quartz crystals were heated to 350 C and then, immediately upon removal from the oven, quenching in cold distilled water. After drying in a vacuum oven at 150 C overnight, inclusion-free quartz crystals were sealed with an arc-welder in Pt capsules along with other starting materials.

In the first experiment, distilled water and a quartz crystal were sealed in a Pt capsule to check crack healing and trapping fluids. In the second experiment, Mg(OH)<sub>2</sub> and a quartz crystal were sealed. In the third experiment, Mg(OH)<sub>2</sub> was sealed with quartz rapped in a Pt foil (0.0025mm in thickness) with holes (30-50  $\mu$ m in diameter) to prevent the reaction between quartz and Mg(OH)<sub>2</sub>. Pt capsules were about the bottom portions of 5 mm long, 2mm in diameter (0.1mm in thickness). The capsules were placed into piston cylinder, solid media apparatus. Experimental conditions were 800 C, 1GPa and 3 hours. After quenching, thick thinsections (60-100  $\mu$ m in thickness) were prepared to examine with a optical microscope and a scanning electron microscope equipped with and energy dispersive X-ray spectrometer.

### Results and discussions

In the observation of the first sample, fluid inclusions with 5  $\mu$ m size were in quartz crystal.

In second sample, fluid inclusions with 5-15  $\mu$ m size were observed in quartz crystal. Mg<sub>2</sub>SiO<sub>4</sub> polycrystal band with 100-200  $\mu$ m thickness was observed between quartz and MgO (or Mg(OH)<sub>2</sub>). Moreover, a few MgSiO<sub>3</sub> crystals were observed between quartz and Mg<sub>2</sub>SiO<sub>4</sub>. Therefore, the reaction between quartz and Mg(OH)<sub>2</sub> were undoubtedly caused during the second experiments.

In third sample, fluid inclusions with 5-15  $\mu$ m size were observed. A little amount of Mg<sub>2</sub>SiO<sub>4</sub> was observed on the points where quartz was not wrapped in Pt foil. However, the reaction between quartz and Mg(OH)<sub>2</sub> were scarcely caused during the third experiments.

### Conclusion

In present study, we trapped dehydrated fluid from hydrated minerals in quartz for the first time. However, 5-15  $\mu$ m was not enough size to estimate the chemical composition of fluid inclusions. Discovery of the experimental condition to synthesize large



fluid inclusions will lead the interpretation about fluids behavior in the subduction zone.

Keywords: fluid inclusion, dehydrated fluid, synthetic experiment, piston cylinder

SCG060-P09

Room:Convention Hall

Time:May 25 16:15-18:45

## Evolution of Microstructure and Flow Properties of Fault in Neogene siliceous Mudstone

Shin-ichi Uehara<sup>1\*</sup>, Miki Takahashi<sup>1</sup>

<sup>1</sup>GSI, AIST

When we evaluate patterns of flow and mass transportation through underground space, fractures and faults in rocks cause severe uncertainties. The uncertainties are partly from those in flow properties of a single fracture or fault. The flow properties of a fault and fracture generally depend on several factors such as intact rock properties or stress conditions. It is therefore important to evaluate dependencies of flow properties through a single fault on several factors, for evaluation of their effects on flow properties of bulk rock mass.

We operated laboratory experiments to measure flow rate through a mudstone specimen during axial deformation under confining pressure, with siliceous mudstone from Koetoi and Wakkanai Neogene Formations, Horonobe, Hokkaido. Main origins of Koetoi and Wakkanai Formation (Fm.) mudstones are the same, fossil diatoms, but phases of amorphous silica are different; at the boundary between these Fms., the phase changes from Opal-A to Opal-CT. Therefore Wakkani Fm. mudstone is denser and harder than Koetoi Fm. mudstone. Japan Atomic Energy Agency (JAEA) has done detail researches relating to flow properties of rock mass at underground situation, including by drilling cores or borehole explorations down to the depth of several hundred meters to a few kilometers in this region. Previous studies indicated that in-situ flow path tends to concentrate at some locations, which seems to match with the locations of faults and fractures in Wakkanai Fm., while, in Koetoi Fm., this tendency is weak. This difference can reflect differences on characteristics of flow properties of faults. Therefore we operated laboratory experiments with these rocks and tried to examine this possibility.

We adopted a specimen arrangement similar to experiments of Takahashi (2003, JGR); we put a cylindrical mudstone specimen of 20mm in length and 20mm in diameter between cylindrical Berea sandstone specimens of 10mm in length and 20mm in diameter. The mudstone specimen is intact, but the sandstone specimens have saw-cut plane of which an angle is 30 degrees with respect to the axis of the specimen. The sandstone specimens are set at the both side of the mudstone specimen so that the saw-cut planes are on the same plane, in order to induce shear zone in the mudstone specimen when axial force is applied. The advantage of this method is that we can see if flow rate along induced shear zone, or fault, is effectively large comparing to the intact part of mudstone.

We set confining pressure and average pore pressure as 8.3 and 4.9MPa, respectively, considering the condition of a depth of approx. 500m in this region. We used distilled water as a pore fluid and operated the experiments under room temperature. We applied an axial displacement with a constant velocity, 0.2um/sec, and measured permeability of the axial direction by oscillation pore pressure method. We used specimens prepared from three locations of the drilling core of HDB 10; 43.2m, 264.0m, (Koetoi Fm.), and 385.0m (Wakkanai Fm.) in depth.

Main results of the laboratory experiments and microstructure observations are as follows. (1) Measured permeability is similar to permeability before deformation, or intact permeability, for Koetoi Fm. mudstone, while, in the case of Wakkanai Fm. mudstone, permeability increases after deformation. (2) Micro focus X-ray computed tomography images of induced shear zones indicated that the shear zone in Koetoi Fm. mudstone is compacted, while that in Wakkani Fm. mudstone is dilative and fractures are observed around the shear zone, which suggested that the shear zone may work as a conduit. The differences of shear zone flow properties in laboratory experiments between two Fms. may be related to differences in observed in-situ flow.

This research is supported by the Ministry of Economy, Trade and Industry of Japan. We express our gratitude to Dr. Niizato, JAEA, for his efforts to prepare drilling core samples from HDB 10.

Keywords: fault flow property, laboratory hydro-mechanical experiment, siliceous mudstone, Horonobe, permeability, micro focus X-ray CT

SCG060-P10

Room:Convention Hall

Time:May 25 16:15-18:45

## An experimental investigation on the fluid distribution in amphibolitic lower crust

Masamichi Abe<sup>1</sup>, Michihiko Nakamura<sup>1\*</sup>

<sup>1</sup>Department of Earth Science TOHOKU Univ.

The connectivity of COH fluids in the polycrystalline aggregates of pargasite, anorthite, and those two was assessed in terms of the geometry of crystal-crystal-fluid triple junction in the synthetic rocks. All the experiments were carried out at 600 degreeC and 0.7 GPa with fluid fraction of 0.1?3%. To estimate the true dihedral angles without a sectioning effect, the effect of surface energy anisotropy was considered using the cumulative frequency curve of the apparent dihedral angle measured on cross sections.

In the anorthite?fluid systems, populations of the curved-curved (CC) type triple junction were ca. 45% irrespective of the fluid composition, whereas their median dihedral angles depend on the fluid composition; 80 degree for H<sub>2</sub>O, 93 degree for CHO and 70 degree for 6 wt.% NaCl aqueous solution. The true CC type dihedral angles, estimated according to the theory of Laporte and Provost (2000), range from 53 to 102 degree. Since most of the dihedral angles is >60 degree in the anorthite aggregate, the intergranular fluid will not be connected as long as the fluid fraction is small. In the pargasite aggregate, the CC type was less dominant; ca. 65% of the triple junction was faceted?faceted (FF) type. It should be noted that most of the FF type were impingement grain boundary. If I assume that the true dihedral angle does not have a single value but constant probability distribution, then its range is calculated to be 28?88 degree. Assuming for simplicity that the pore geometry is equilateral triangular pyramidal, the true dihedral angle has this range when the ratio of hypotenuse to base of the pyramid is 0.7?5.6. This simple model shows that the pyramid of pore fluid in the pargasite aggregate has a finite height and will not be interconnected, because if the fluid is interconnected, its geometry approaches a tube lacking the base plane and the maximum value of the true dihedral angle (formed only with two side faces) is less than 60 degree. In the anorthite-pargasite-fluid system, the population of the triple junction consisting of a curved anorthite and a faceted pargasite faces is >65%. It is calculated that the true dihedral angle of this type of triple junction has a range of 31?57 degree on the basis of the cumulative frequency curve of the measured apparent dihedral angle.

The FE-SEM observation showed that most of the FF and FC type boundaries were formed by impingement, and thus surface tensions at these grain boundaries were not balanced. However, such boundaries were stable as long as the experimental duration. In addition, it is observed that the impingement grains are common in natural amphibole or biotite in the high-grade metamorphic rocks. Therefore, the pore geometry determined by the impingement grains seem to represent a stable structure. Judging from the observed pore-type populations, the FFC and FCC type pores are most likely in the amphibolitic aggregate. The connectivity of these types of pore are relatively high, because the FC type dihedral angle is relatively low (31 - 57 degree) even at the small fluid fraction of the present experiments and the curvature can be continuous along the curved grain boundary (von Bargen and Waff, 1986). The fluid may be interconnected along the edges surrounded by the faceted plane(s) and curved edge(s). The possibility of interconnection at the grain corners is also high. Thus, the connectivity of fluid in the aggregates of amphibole and anorthite is strongly dependent on the modal composition.

Keywords: continental lower crust, low electrical resistivity, interconnected fluid, dihedral angle, surface energy anisotropy

SCG060-P11

Room:Convention Hall

Time:May 25 16:15-18:45

## Experimental study on calcite precipitation in hydrothermal environments

Michimasa Musha<sup>1\*</sup>

<sup>1</sup>Tohoku Univ.

The crustal fluids are commonly characterized by the compositions in C-H-O system, mainly composed of H<sub>2</sub>O, CO<sub>2</sub> and CH<sub>4</sub>, and thus transport of these fluids and precipitation of carbonate are important for the global carbon cycle. To reduce greenhouse gas (CO<sub>2</sub>, CH<sub>4</sub> etc) in the atmosphere, the carbon storage underground has been tried; however, it is considered to be difficult to precipitate calcite in reasonable timescale. In contrast, calcite veins are very common in the oceanic crusts, metamorphic rocks, and accretionary prisms. For example, calcite + quartz veins occur ubiquitously in the Shimanto belt. The solubility of calcite decreased with temperature, that is the opposite trend of quartz; and thus how calcite precipitated in the conditions that quartz also occurs is puzzling. In spite of its importance, the experimental studies on the calcite precipitation are very limited. Most experiments are carried out under near room temperature and controlled by pH change or synthetic CO<sub>2</sub> saturated fluids (Lee & Morse, 1999), that are far from natural conditions of calcite-vein formation. To best of our knowledge, there are no experimental studies on calcite precipitation under hydrothermal conditions (>100 degree C).

The purpose of this study is to understand the controlling factors on calcite precipitation under conditions of calcite-vein formation (fluid compositions, P-T conditions, host rock types). The solubility of calcite increases with decreasing temperature, with increasing fluid pressures, and with increasing concentration of NaCl (Ellis, 1963). What is the most controlling factor that enhances the calcite-vein formation at the conditions of the Shimanto belt is unknown. As a first step, we conducted hydrothermal flow-through experiments to precipitate calcite at 300 degree C and 30 MPa by using the temperature dependency of solubility.

Before the precipitation experiments, because a reliable solubility data on calcite at elevated temperature is lacking, we tested how amount of Ca ions dissolved from calcite in the flow-through system at 30 MPa with temperature range from 100 to 400 degree C. The Ca concentration path-through the vessel is highest at 100 degree C, and it decreased with increasing temperature.

The experimental apparatus of the precipitation experiments is composed of two reaction vessels; in the first vessel, the super-saturated solutions were prepared by dissolution of limestone sand (1-2 mm in size) in the distilled water at 100 degree C. In the second vessel, seven limestone substrates (5x5x15 mm) were set along the flow-path. The limestone is composed of fine grained aggregate of calcite (<0.03 mm). The temperature of the precipitation vessel was set to be 300 degree C. The fluid flow rate was 1 ml/min. After the run of 240 h (10 days), the total increase of weight of limestone substrates was 0.051 g. Observation of the surface morphologies of the substrates by SEM and thin sections by optical microscope reveal that euhedral calcite crystals with size of 0.02-0.03 mm grew from the calcite in the substrates.

Our results suggest that calcite veins could be formed around 300 degree C, if fluids saturated with calcite at lower temperature would be brought accompanying with subduction of slabs. However, our experimental conditions deviate from that of quartz and calcite vein formation, because the temperature increase leads to the dissolution of quartz, so that it cannot be co-existing of quartz and calcite in the same veins. Second, the source of Ca and CO<sub>3</sub><sup>2-</sup> would be the host sedimentary or basaltic rocks in the Shimanto belt. We will try to precipitate calcite with using other factors, including pressure dependence on the solubility, the host rock type.

References: Lewis J. C., Byrne T. B., J.D.Pasteris, (2000), *J. metamorphic Geol.*, 2000, 18, 319-333

Y. J. Lee, J. W. Morse, (1999), *Chemical Geology*, 156 (1999), 151-170

A. J. Ellis, (1963), *American Journal of Science*, 261, 1963, 259-267

Keywords: accretionary prism, subduction zone, calcite, mineral veins

SCG060-P12

Room: Convention Hall

Time: May 25 16:15-18:45

## Optical pressure sensors for DAC experiment: application in high-pressure studies

Nadezda Chertkova<sup>1\*</sup>, Shigeru Yamashita<sup>2</sup>

<sup>1</sup>ISEI, Okayama University, <sup>2</sup>ISEI, Okayama University

Structural properties of melts and minerals are widely examined by in situ spectroscopic studies with externally heated diamond anvil cell (HDAC) [1]. While the temperature can be controlled with an accuracy of plus/minus 0.5-1.5 degree C with this technique [2], a direct pressure measurement is complicated by the differences in compressibility and thermal expansivity for the variety of samples. Only few spectroscopic standards can be used for pressure determination in the HDAC experiments involving silicate melts. One of the non-reactive pressure sensors which was calibrated in the wide pressure- and temperature ranges is <sup>13</sup>C diamond [3]. Its first-order Raman shift is distinct from that of diamond anvils and indicates the pressure in immediate proximity to the sample.

The objective of this work was to test the precision of <sup>13</sup>C diamond pressure marker at high pressures and elevated temperatures. Experiments were carried out in the HDAC, with pure H<sub>2</sub>O as a pressure medium and two optical pressure markers - <sup>13</sup>C diamond aggregate chip and ruby chip. Already well established phase transitions in H<sub>2</sub>O system and ruby fluorescence pressure scale were used as references for checking the precision of pressure determination with <sup>13</sup>C diamond Raman shift.

In the temperature (22-300 degree C) and pressure (up to 4.8 GPa) ranges studied, a good agreement between the phase transitions in H<sub>2</sub>O system and the pressure values obtained from two pressure sensors was achieved during heating cycles. The average difference between pressures calculated from <sup>13</sup>C diamond Raman shift and those calculated from ruby fluorescence line shift (0.16 GPa) lies within the reported uncertainty of calibrations [3], [4], [5]. The largest full width at half-maximum (FWHM) for the first-order Raman peak of <sup>13</sup>C diamond was found to be approximately 9.9 cm<sup>-1</sup> at 300 degree C, that is much smaller than FWHM for ruby fluorescence lines.

Experiments in the H<sub>2</sub>O system demonstrated that <sup>13</sup>C diamond is a precise pressure sensor which immediately detects sudden pressure drops in the case of sample decapsulation. These features are essential for the pressure control in in-situ studies of magmatic phenomena, such as mixing behavior of magma and volatiles, structural changes in melts and fluids, crystallization sequences.

### References

1. Smith R.L. and Fang Zh. (2009) Techniques, applications and future prospects of diamond anvil cells for studying supercritical water systems. *Journal of Supercritical Fluids*, V. 47, P. 431-446.
2. Bassett W.A., Shen A.H., Bucknum M., and Chou I.M. (1993) A new diamond cell for hydrothermal studies to 2.5 GPa and from -190 degree C to 1200 degree C. *Reviews of Scientific Instruments*, V. 64, P. 2340-2345.
3. Schiferl D., Nicol M., Zaug J.M., Sharma S.K., Cooney T.F., Wang S.-Y., Anthony T.P., Fleischer J.F. (1997) The diamond <sup>13</sup>C/<sup>12</sup>C isotope Raman pressure sensor system for high-temperature/pressure diamond-anvil cells with reactive samples. *Journal of Applied Physics*, V. 82, P. 3256-3265.
4. Zha C.S., Mao H.K., and Hemley R.J. (2000) Elasticity of MgO and a primary pressure scale to 55 GPa. *PNAS*, V. 97, P. 13494-13499.
5. Ragan D.D., Gustavsen R., Schiferl D. (1992) Calibration of the ruby R<sub>1</sub> and R<sub>2</sub> fluorescence shifts as a function of temperature from 0 to 600 K. *Journal of Applied Physics*, V. 72, P. 5539-5544.

Keywords: diamond anvil cell, <sup>13</sup>C diamond, ruby, pressure sensor

SCG060-P13

Room:Convention Hall

Time:May 25 16:15-18:45

## Seismic velocities of crustal rocks and minerals

Kyoko Matsukage<sup>1\*</sup>, Yu Nishihara<sup>2</sup>

<sup>1</sup>GRC, Ehime University, <sup>2</sup>SRFC, Ehime University

Recently, seismologists obtain high-resolution data of crust and mantle on distribution of seismic wave velocities (e.g., Nakajima et al., 2001). For interpretation the origin of distribution of seismic wave velocities, we have to know the relation between chemical variation and its seismological signature. There are two methods to obtain the relation. The first is direct seismic velocities measurement of bulk rock (multi-phases sample) by using high-pressure apparatus (e.g., Nishimoto et al. 2008; Kono et al. 2009). The second is theoretical calculation by using the data of well-defined thermoelastic parameters of minerals and modal composition. We can calculate the seismic velocities of rocks at various temperatures and pressures in the Earth's interior if some important thermoelastic parameters of constituent minerals, such as bulk modulus, its pressure derivative, density, Debye temperature, Gruneisen parameter, shear modulus and its pressure derivative at room pressure and temperature are obtained. Recently, we can obtain reliable thermoelastic parameters of upper mantle minerals by literatures in wide pressure and temperatures range, which cover the whole upper mantle of the Earth (e.g., compiled by Matsukage et al., 2005). Therefore the calculated seismic velocities of mantle rocks such as lherzolite and harzburgite can be compared directly with the seismic velocities profiles observed by seismologists (e.g. PREM, AK135).

On the other hand, the thermoelastic parameters of crustal minerals (e.g., amphibole and plagioclase) are not determined very well because of at least two experimental difficulties. The first problem is the low symmetric crystal structure of crustal minerals. The second problem is the narrow stability field, less than  $\sim 3$  GPa and  $\sim 1300$  K. In this study, we try to calculate the thermoelastic parameters of crustal minerals by using the P-V-T equation of state data and heat capacity measured by previous studies, and estimate the seismic velocities of gabbroic and eclogite rocks with various chemical compositions at high-pressure and high-temperature. We also try to measure the elastic wave velocities and density (P-V-T data) of plagioclase and amphibole by using the multi-anvil apparatus with synchrotron X-ray in SPring-8. In this presentation, we are going to discuss the reliability of the calculation and show the relation between chemical variation of crustal rocks and its seismological signature.

Keywords: seismic velocity, gabbro, eclogite, plagioclase, amphibole, pyroxene



SCG060-P14

Room:Convention Hall

Time:May 25 16:15-18:45

## Seismic Velocity Structure beneath Kii Peninsula

Taishi Fukui<sup>1\*</sup>, Takuo Shibutani<sup>1</sup>, Setsuro Nakao<sup>1</sup>, Kazuhiro Nishimura<sup>1</sup>, Masayo Sawada<sup>1</sup>, Kazuro Hirahara<sup>2</sup>

<sup>1</sup>DPRI, Kyoto Univ., <sup>2</sup>Science, Kyoto Univ.

Philippine Sea Plate is subducting beneath the southwest Japan arc from the Nankai Trough. This causes megathrust earthquakes in the subduction zone. The latest events along the Nankai Trough are Showa Tonankai Earthquake (M7.9) in 1944 and Showa Nankai Earthquake (M8.0) in 1946. The next event is predicted to occur in 2030 - 2036 (Earthquake Research Committee, 2001). It is thought that the surrounding area of the southern edge of Kii Peninsula is most likely to be a rupture starting point of the megathrust events as it was in the Showa events. At the same time, the Kii Peninsula is a region through which hazardous seismic waves propagate from the megaquakes to large cities such as Osaka, Kyoto and Nara. The purpose of this study is to estimate structure of seismic velocity discontinuities, especially slab configurations beneath the Kii Peninsula. This is very important to upgrade the ways of predicting megaquake generations and strong motions caused by the events.

We have carried out linear array seismic observations in the Kii Peninsula since 2004. We deploy temporary seismic stations in the vicinity of profile lines with an average spacing of ~5 km and a length greater than 80 km (Fig. 1). We obtain images of seismic velocity discontinuities beneath the Kii Peninsula by using a receiver function analysis with teleseismic waveforms, and estimate structure of the subducting slab and the surrounding regions in detail. We have completed the observations and analyses for three profiles in the subduction direction (Shiono Cape - Tajiri Line AA', Shingu - Kawachi-nagano Line BB', Owase - Kyotango Line CC') so far. As a result, the upper surface of the low velocity oceanic crust (the upper surface of the Philippine Sea slab), the oceanic Moho in the slab and the continental Moho in the arc side were clearly imaged. Furthermore, strong low velocity anomalies were found in the vicinity of the slab in the generating area of the deep low frequency events and widely in the mantle wedge.

We redeployed temporary stations along three profile lines in March 2009. One is Minami-ise - Shigaraki Line DD' in the subduction direction and the others are Matsuzaka - Shirahama Line EE' and Kameyama - Gobo Line FF' in the perpendicular direction.

We estimated the depth contours for the continental Moho, the upper surface of the oceanic crust and the oceanic Moho by combining depth data of the discontinuities beneath the six survey lines picked up on the receiver function images.

In this presentation we will introduce the linear array seismic observation in the Kii Peninsula, the estimated features of the Philippine Sea slab configuration and the mantle wedge structure and the features of the contour maps of the three discontinuities.

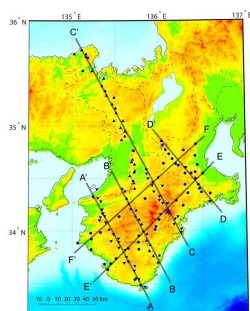


fig1. Seismic observation stations in the Kii Peninsula ▲, ●.  
Survey lines(AA', BB', CC', DD', EE', FF') are solid lines in the map.

Keywords: philippine Sea slab, Mantle wedge, Receiver function image, Linear array seismic observation, Kii Peninsula

SCG060-P15

Room:Convention Hall

Time:May 25 16:15-18:45

## Receiver function imaging of the Philippine Sea slab beneath Kyushu, southwest Japan

Yuki Abe<sup>1\*</sup>, Takahiro Ohkura<sup>1</sup>, Kazuro Hirahara<sup>2</sup>, Takuo Shibusaki<sup>3</sup>

<sup>1</sup>AVL, Kyoto Univ., <sup>2</sup>Graduate School of Science, Kyoto Univ., <sup>3</sup>DPRI, Kyoto Univ.

In subduction zones, the subducting slabs are thought to convey fluid into the mantle wedge and to cause arc volcanism. It is revealed that serpentinized layer in the mantle wedge beneath NE Japan subducts along the Pacific slab, releases its fluid at about 150 km in depth, and the released fluid moves to the volcanic front, with seismic tomography, receiver function (RF) analysis and geochemical simulation (Hasegawa et al., 2008; Iwamori, 2007; Kawakatsu & Watada, 2007). Oceanic plates subducting beneath Kyushu (west Philippine Sea basin: 50Ma. Shikoku basin: 27Ma) are younger than the Pacific plate subducting beneath NE Japan (130Ma), and an island arc crust, Kyushu-Palau ridge, is subducting beneath Kyushu. The mantle wedge structure beneath Kyushu has been estimated and fluid distribution has been elucidated by tomographic studies (Zhao et al., 2000; Honda & Nakanishi, 2003; Wang & Zhao, 2006). It is revealed that the subducted oceanic crust exists at 60 km in depth and the Philippine Sea slab (PHS) conveys fluid down to this depth beneath the central part of Kyushu (Okamoto et al., 2008). However, it has not been elucidated where the hydrated portion extends along PHS. It is important to estimate the structure of PHS and reveal hydrated portion for better understanding of fluid transportation by a young slab. We estimate the geometry of seismic velocity discontinuities of PHS with RF analysis.

We use 439 teleseismic waveforms (origin time: Aug.1996-Feb.2009, epicentral distance: 30-90°, magnitude: greater than 5.5) observed at 78 Hi-net stations and 61 J-array stations. Transverse RFs which hail from the southeast are constructed with the extended-time multitaper method (Shibusaki et al., 2008). We use the fast-marching method (de Kool et al., 2006) to stack RFs with taking account of refraction at dipping interfaces (Abe et al., submitted). RFs are stacked in a region (31-34°N, 129-132°E and 0-300 km in depth), which includes the Wadati-Benioff zone of PHS beneath Kyushu, and projected on sections perpendicular to the strike of PHS. We assume a 1-d model of ak135 (Kennett et al., 1995), and stack RFs several times with assuming varying geometries of conversion surfaces, so that the assumed interface geometry coincides with that obtained from RF sections.

We obtain discontinuities with upward decreasing velocity along the Wadati-Benioff zone of PHS. These discontinuities extend to 80-150 km in depth. Discontinuities with upward decreasing velocity along a slab are expected to be the oceanic Moho or the bottom interfaces of serpentinized mantle (Kawakatsu & Watada, 2007). Since these obtained discontinuities extend up to 150 km, shallower and deeper portions of them are interpreted as the oceanic Moho and the bottom interfaces of serpentinized mantle, respectively, although we do not distinguish the two interfaces. Therefore, these discontinuities are expected to be the bottom of hydrated portion, and fluid transportation along PHS is revealed.

We obtain discontinuities which are interpreted as the top surface of PHS only in the region, at 32°N, 60-80 km in depth. They might be the top surface of the island arc crust (Kyushu-Palau ridge), and the structure of this region should be examined more in detail. Discontinuities interpreted as the top surface of PHS do not detected beneath the other region. This fact indicates that seismic velocity contrast at the top surface of PHS is small, and is consistent with the fact that the fore-arc mantle wedge has low seismic velocity (Zhao et al., 2000; Honda & Nakanishi, 2003; Wang & Zhao, 2006).

We use waveform data observed by the National Research Institute for Earth Science and Disaster Prevention, Kyushu Univ., Kagoshima Univ. and Japan Meteorological Agency, and hypocentral data collected by Japan Meteorological Agency. We use FMTOMO (de Kool et al., 2006) to calculate travel time fields with the fast-marching method.

Keywords: receiver function, Philippine Sea slab, Kyushu, fast-marching method

SCG060-P16

Room:Convention Hall

Time:May 25 16:15-18:45

## 3D electrical resistivity modeling of the Onikobe caldera -Implications for volcanoes and earthquake activity

Hiromi Fukino<sup>1</sup>, Yasuo Ogawa<sup>2\*</sup>, Masahiro Ichiki<sup>3</sup>, Wataru Kanda<sup>2</sup>, Bulent Tank<sup>4</sup>

<sup>1</sup>EPS, Titech, <sup>2</sup>KSV0,Titech, <sup>3</sup>Tohoku Univ., <sup>4</sup>Bogazici Univ.

The Onikobe caldera is an oval topographic depression of 7.5km x 10km. In its southern part, there are active geothermal fields in east-west directions and the most active geothermal manifestation Katayama-Jigoku is in its southeastern end. Around the area, many crustal earthquakes occur, such as Iwate-Miyagi Nairiku Earthquake(Mw 6.9). The objective of this study is to image the resistivity structure in three dimensions in order to relate the distribution of fluids to volcanoes and earthquakes.

MT survey of 30 sites was conducted in 2009 in and around the Onikobe caldera. Three-dimensional inversion (WSINV3DMT) was applied to the dataset using the full impedance components. The results of the inversions are as follows. A low resistivity body with north-south strike was found at 20km depth in the western part of the caldera. The conductor extends upward, but it starts to branch laterally at 15km depth. One minor branch goes to 3km depth under the Mukaimachi caldera, which is located to the south-west of Onikobe caldera. Another major conductive branch reaches 2km depth below the surface of Katayama-Jigoku. The latter conductor has an east-west strike, which reflects the regional direction of tectonic compression. The resistivity of such crustal anomaly is between 1 and 10 ohmm. Using the Hashin-Strikman model, where conductive fluid shells cover the resistive rock matrix, the conductors will have fluid content as 1-7%, if we assume typical saline crustal fluids. Earthquakes occur at resistive zone above conductive body. This suggests the triggering of earthquake by fluids.

Keywords: magnetotelluric, inland ?earthquake, geofluid

SCG060-P17

Room:Convention Hall

Time:May 25 16:15-18:45

## The effect of heat and fluid on dynamic earthquake rupture in inhomogeneous stress field

Ryo Itoh<sup>1\*</sup>, Takehito Suzuki<sup>2</sup>, Satoshi Ide<sup>2</sup>

<sup>1</sup>ERI, Univ. Tokyo, <sup>2</sup>EPS, Univ. Tokyo

We numerically investigate the effect of the interaction among heat and fluid on dynamic fault tip growth. The interaction, referred to as thermal pressurization (TP), is briefly summarized as follows. When fault slip occurs, frictional heat source appears and it raises fluid pressure. The high-pressured fluid reduces effective normal stress acting on the fault plane, which reduces the frictional stress. This frictional stress reduction enhances the fault slip and the heat source term is again changed. TP is therefore regarded as positive feedback in dynamic fault slip process. Though this mechanism has been studied widely, there has been a problem that many researchers have assumed homogeneous model setup. Natural faults show inhomogeneity in many aspects such as material properties and stress field. For example, the slab beneath Tohoku shows compression (upper zone) and tension (lower zone) stress field and earthquakes are observed to propagate in such stress field. In addition, fluid dehydrated from rocks is believed to exist in and around the slab and it is expected that TP works strongly in the region. We should therefore consider how TP works in inhomogeneous stress field.

We assume dynamic fault tip growth in a thermoporoelastic medium; thermoporoelastic medium has been assumed by a number of researchers to treat TP. Spontaneous fault tip growth with the Coulomb fracture criterion is assumed. Shear stress acting on the fault plane is assumed to decrease linearly with distance from the rupture nucleation point, which generates the region where the shear stress acts in the opposite direction. We can therefore expect that the fault tip growth is arrested spontaneously if we do not consider TP.

The fault tip with TP is found in our calculations to extend to the region where the shear stress changes its direction from the nucleation point, which occurs because of the positive feedback due to TP. If the spatial change rate of the shear stress is smaller, the fault tip can grow further. The results obtained here may explain the reason that earthquakes occurring in, for example, the Tohoku slab can extend over both compression and tension regions.

Keywords: fluid, heat, inhomogeneous stress field, slab, dynamic earthquake rupture

SCG060-P18

Room:Convention Hall

Time:May 25 16:15-18:45

## Heterogeneity beneath Japan as inferred from energy partitioning of P-wave and implication for seismic radial anisotropy

Mare Yamamoto<sup>1\*</sup>

<sup>1</sup>Geophysics, Science, Tohoku University

Seismic radial anisotropy is generally attributed to horizontal layering (especially with thin fluid layer and fluid-filled cracks) and/or large-scale deformation in the lower crust and upper mantle, and it has been extensively studied by surface wave analyses in order to elucidate geodynamical processes and fluid circulation. However, use of surface waves having long wavelength makes it rather difficult to discriminate between solid-fluid layering and TI anisotropy of the media. On the other hand, it is also known that the short-wavelength heterogeneity in the crust and upper mantle causes the scattering phenomena of high-frequency seismic waves such as the excitation of transverse component of teleseismic P-wave.

In this study, by systematically analyzing the excitation of transverse component of P-wave observed at NIED Hi-net stations, we map spatial variation of the heterogeneity beneath Japanese island and examine the detectability of radial anisotropy. We also compute the wave scattering in anisotropic random media using the finite difference method, and study the dependence of excitation of transverse component to the propagation direction.

In the data processing, for each frequency band, we calculate the energy partition of direct P-wave into the transverse component at each station. After averaging over events with different incident azimuthal direction and incident angle, spatial variation of the normalized transverse energy shows consistent feature with the tomographic image and spatial variation of coda-Q. This result suggests that the observation of energy partition is a good measure to characterize the structural heterogeneity. On the other hand, the normalized transverse energy also shows dependence to the incident angle, which cannot be explained by wave propagation in simple isotropic random media. To understand the cause of the angular dependence of the normalized transverse energy, we conducted finite difference modeling of the wave scattering due to anisotropic random media and examine the effects of incident angle. The results of numerical modeling indicate that the observed characteristic can be explained by oblique propagation of P wave into anisotropic random media having longer correlation distance in horizontal directions. These results imply that it may be possible to have new insight into the cause of radial anisotropy, deformation field, and fluid distribution beneath Japanese island.

Acknowledgment: I used Hi-net data provided by the National Research Institute for Earth Science and Disaster Prevention.

Keywords: Seismic wave propagation, Seismic wave scattering, Geofluid

SCG060-P19

Room:Convention Hall

Time:May 25 16:15-18:45

## Estimation of corner frequency using the spectral ratio method and attenuation structure beneath NE Japan

Shuhei Hada<sup>1\*</sup>, Junichi Nakajima<sup>1</sup>, Naoki Uchida<sup>1</sup>, Erika Hayami<sup>1</sup>, Norihito Umino<sup>1</sup>

<sup>1</sup>Tohoku University

Seismic attenuation is sensitive to temperature, water content, chemical composition and partial melting in a different way from that of velocity. Hada et al. (2010) estimated 3-D attenuation structure beneath northeastern (NE) Japan, using the method of Eberhart-Phillips and Chadwick (2002). In this method, spectra of waveforms from local earthquakes were used to determine simultaneously whole ray path attenuation terms,  $t^*$ , spectral level,  $c_0$  and corner frequency,  $f_c$ . However, it is difficult to estimate accurate  $t^*$  because of a strong trade-off between  $t^*$  and  $f_c$ . Here, we estimate an exact value of  $f_c$  of each earthquake, using the spectral ratio method, and determine  $t^*$  precisely for each event-station pair.

We apply Multi-window Spectral Ratio method (Imanishi and Ellsworth, 2006) to S-wave coda, instead of direct waves, to obtain more stable spectral ratios. This method can remove the effects of a radiation pattern of source mechanism, site amplification, and heterogeneous structure. We analyzed 641 intraslab earthquakes ( $M > 2.5$ ) beneath NE Japan for the period from 2006 to 2009. Waveforms were recorded at a nation-wide seismograph network with a sampling frequency of 100 Hz. First, spectral ratios of two earthquakes were calculated for common stations for five moving windows by overlapping half duration of each window length of 0.25s. All the calculated spectral ratios were then stacked, and  $f_c$  of each earthquake was estimated by fitting the average spectral ratio to an omega-squared source model at frequency ranges of  $S/N > 3$ . Finally,  $t^*$  of each event-station pair was estimated from the decay of spectrum at higher frequencies than  $f_c$ .

The obtained results show that  $f_c$  and  $t^*$  are estimated more precisely than by Hada et al. (2010). Estimated corner frequencies follow cube-root scaling with seismic moment and 0.1-10 MPa stress drop. In addition,  $t^*$  calculated for adjacent earthquakes are very similar to each other, indicating the stability of our strategy used in this study. Estimated  $t^*$  shows a prominent along-arc variation with small  $t^*$  (low attenuation) in the fore arc and high  $t^*$  (high attenuation) in the back arc, which probably reflect the difference in the nature of the mantle wedge structure. In the next step, we will perform tomographic inversion using the calculated  $t^*$  and estimate 3D seismic attenuation structure to understand ongoing subduction-zone processes in the mantle.



SCG060-P20

Room: Convention Hall

Time: May 25 16:15-18:45

## Estimation of the stress field and the pore-pressure from focal mechanisms in the focal area of the 2008 IMNE

Keisuke Yoshida<sup>1</sup>, Tomomi Okada<sup>1</sup>, Yoshihiro Ito<sup>1\*</sup>, Takeshi Inuma<sup>1</sup>, Norihito Umino<sup>1</sup>, Akira Hasegawa<sup>1</sup>, Group for the after-shock observations of the Iwate-Miyagi Nairiku Earthquake<sup>2</sup>

<sup>1</sup>RCPEV, <sup>2</sup>GIMNE2008

### 1. Introduction

The 2008 Iwate Miyagi Nairiku earthquake with a magnitude of 7.2 occurred in the southwest part of Iwate Prefecture and northwest part of Miyagi Prefecture on June 14, 2008. Previous studies have revealed the aftershock distribution, coseismic and afterslip distribution, and seismic wave velocity structure. These studies suggest that crustal fluid may had influence of the occurrence of the mainshock.

In this study, we estimated the stress field before and after the mainshock, and pore-pressure distribution after the mainshock using the data recorded by the routine stations of Tohoku University, JMA, Hi-net-NIED, and temporal stations by the Japan Nuclear Energy Safety Organization and the Group for the aftershock observations of the Iwate-Miyagi Nairiku Earthquake in 2008.

### 2. Estimation of the stress field

First, we divided the data set into into 2 subsets before (1998-2008/6/14) and after the mainshock (2008/6/14-9/30), and we estimated the stress field by the stress tensor inversion (Abers and Gephart, 2001) using first motions of the earthquakes. Before the mainshock, the maximum principal stress ( $\sigma_1$ ) direction seems to orient ESE-WNW or E-W.  $\sigma_1$ -direction seems to orient E-W especially in the south of the focal area. These directions are consisted with the average directions of the P-axis of the focal mechanisms of the earthquakes in each area before the mainshock. The minimum principal stress ( $\sigma_3$ ) axes are horizontal in the east areas, but perpendicular in the west areas. These directions are consisted with the directions of the principal strain rate in each area. (Miura et al., 2004)

After the mainshock, stress field have some varieties in the local scale (5-10km) in the focal areas.  $\sigma_1$  direction are NW - SE in the east areas, but NE - SW in the shallow part (0-2 km) of west areas, and E-W in the south areas. These directions are consisted with the average directions of the P-axis of the focal mechanisms of the earthquakes in each area after the mainshock. Other areas have WNW-ESE directions of  $\sigma_1$  axis. These change of the  $\sigma_1$  directions before and after the mainshock can be explained by the stress change caused by the mainshock slip if we assume the low values of the deviatoric stress ( $(\sigma_1 - \sigma_3) / \sigma_3 \sim 1.025$ ).

### 3. Estimation of the spatial distribution of the pore pressure

By assuming that the weakening of the frictional strength is caused by the pore-pressure, we estimated the frictional strength (Rivera and Kanamori, 2004) and the pore-pressure distribution by using the aftershock data. High pore-pressure is estimated in the western and northern parts of the focal area. S wave velocity is low beneath these high pore-pressure areas (Okada et al., 2009, 2011). The region of the high pore-pressure zone is also consisted with the spatial extent of the large coseismic and after slip (Inuma et al., 2009). These consistencies may suggest that the overpressurized fluid from the deeper part is redistributed due to the fault slip and weaken the frictional strength of the fault plane in the west area of the focal areas.

Keywords: focal mechanism, stress, pore pressure